International Journal of Medical Physics, Clinical Engineering and Radiation Oncology, 2024, 13, 1-15
https://www.scirp.org/journal/ijmpcero
ISSN Online: 2168-5444
ISSN Print: 2168-5436

Dual-Fields Rotational Total Skin Electron Therapy: Investigation and Implementation

M. Ming Xu[1], Iris Rusu[2], Richard P. Garza[3]

[1]Northwestern Medicine Cancer Center, Warrenville and Geneva, Illinois, USA
[2]Department of Radiation Oncology, Loyola University Medical Center, Maywood, Illinois, USA
[3]The Austin Center for Radiation Oncology, Austin, Texas, USA
Email: Michael.Xu@nm.org

How to cite this paper: Xu, M.M., Rusu, I. and Garza, R.P. (2024) Dual-Fields Rotational Total Skin Electron Therapy: Investigation and Implementation. *International Journal of Medical Physics, Clinical Engineering and Radiation Oncology*, **13**, 1-15.
https://doi.org/10.4236/ijmpcero.2024.131001

Received: November 21, 2023
Accepted: February 15, 2024
Published: February 18, 2024

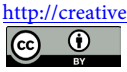

Abstract

Purpose: To present a protocol of a dual-field rotational (DFR) total skin electron therapy (TSET) and to provide an assessment of clinical implementation, dosimetry properties, and skin dose evaluation. **Methods and Materials:** The DFR-TSET combined the Stanford 6-field and McGill rotational methods. Dual 6 MeV electron beams in high dose total skin electron mode were used for DFR-TSET on a commercial linac. Beam profiles and dosimetric properties were measured using solid phantoms. The dose rate at expanded source-to-surface distance (SSD) was a combination of static rate and rotational rate. *In vivo* dosimetry of patient skin was performed on patients' skin using film, metal oxide semiconductor field-effect transistors (MOSFET), and optically stimulated luminescent dosimeters (OSLD). **Results:** Dual field rotational total skin electron therapy exhibited good (≤±10%) uniformity in the beam profiles in the vertical direction at an extended SSD of 332 cm with a gantry angulation of ±20˚ deviated from the horizontal direction. *In-vivo* measurements confirmed acceptable uniformity of the patients' total body surfaces and revealed anatomically self-blocked or shielded areas where under- dosing occurred. **Conclusions:** The clinical implementation of DFR-TSET effectively utilizes the special mode on a linac. This technique provides short beam-on times, uniform dose distribution, large treatment field, and reduced dose of x-ray contamination to the patients. *In-vivo* measurements indicate satisfactory delivery and dose uniformity of the prescribed dose. Electron boost fields are recommended at normal SSDs to address underdosed areas.

Keywords

Total Skin, Electron Therapy, Stanford 6 Field, McGill Rotation Therapy, *In-Vivo* Dosimetry

1. Introduction

Total Skin electron therapy (TSET) or Total Skin Electron Irradiation therapy (TSEI) has been used for many years to treat mycosis fungoides [1]-[10]. Stanford-based Karzmark *et al.* developed a widely used static dual-beam, six-position called Stanford method for TSET [1] [2] [3]. This technique involves positioning six oblique electron beams 60˚ apart around the patient. Each field consists of two component beams angled with respect to the horizontal plane. Treatment using this method requires delivering three beams on the first day and three beams on the second day, completing the prescribed dose over two days [4] [5]. McGill based Podgorsak *et al.* developed rotational total skin electron therapy (RTSET) using a horizontal beam [6]. Compared to the static position Stanford method, the main advantage of the McGill rotational method is the significantly shorter beam-on time, allowing for faster treatment completion [6] [7] [8]. Alternative techniques, such as the translational approach [9], involve translating the patient on a stretcher through an electron beam wide enough to cover the patient's transverse dimensions. Finally, the helical arc radiotherapy has also been used for TSET [10]. All these techniques have been clinically implemented for TSET treatment. Recently, the radiation oncology community has renewed interest in this area [11]-[25].

While the dual-field rotational total skin electron therapy technique has been published previously, [12] [13] [14] [16] [26] [27] the comprehensive implementation of the dual-field rotational total skin electron therapy (DFR-TSET) is largely unknown in the clinic, especially in terms of detailed dosimetry calculations and *in-vivo* dose investigations. With all technologies, achieving uniform dose distribution in the superficial layer of the patient's skin while limiting x-ray contamination is a technical challenge. DFR-TSET may provide such advantages in terms of unique treatment setup, geometries evaluation, and patient shielding for enhanced clinical relevance.

A Varian 21EX or TrueBeam linear accelerator offers a fast electron-beam rate in the high dose total skin electron (HDTSe) mode for TSET [28] [29] [30]. Instead of using a tertiary electron cone, the HDTSe mode can be activated using a special insert provided by the vendor. This mode can produce an electron beam with a nominal rate of up to 2500 MU/min at a source-to-surface distance (SSD) of 100 cm, and a lower dose rate at 100 cm SSD can also be utilized. In this HDTSe procedure, the use of electronic cone inserts is not required with this HDTSe clinically for a patient treatment.

This report describes the development and clinical implementation of the DFR-TSET technique, which combines the advantages of a total dual electron field for TSET with the rotational method. A detailed description of the development of the DFR-TSET technique is provided contributing to the existing knowledge in the area. Additionally, data from *in-vivo* dosimetry measurements are presented to verify dose conformity and uniformity in the DFR-TSET technique. These measurements provide insights into the effectiveness and accuracy

of the technique in delivering the intended dose distribution to the skin. Detailed information, clinical protocols, setup, beam characteristics, and dosimetry, and *in-vivo* dosimetry measurements serve as a reference for future research and clinical implementations.

2. Methods and Materials

2.1. System Set up

A Varian linear accelerator with HDTSe mode was utilized to deliver 6 MeV electron beams for the treatment. No scatters or degraders were placed in front of the patient. To achieve a larger field for a single beam, the source-to-surface distance (SSD) was extended from the 100 cm SSD isocenter by 232 cm, resulting in a 332 cm SSD and a field size of 133 cm by 133 cm. A combined dual electron field with gantry angles of 70˚ and 110˚ relative to the horizontal (90˚) were used to cover the vertical length of 242 cm. The schematic view of the treatment geometry is shown in Figure 1, with the phantom anterior surface located 232 cm from the 100 cm isocenter.

A custom-made rotational platform was used, rotating at a speed of 1.11 revolutions per minute (rpm). The speed of rotation was critical and affected the rotational dose rate and the dose absorbed by the superficial layer. A speed of 1.11 rpm appeared comfortable and tolerated by patients. Patients stand on the rotational platform at an extended SSD of 332 cm. The gantry angles of 70˚ and 110˚ were chosen to ensure that the beams could point above the patient's head and below the patient's feet, respectively. Daily treatments with a machine rate

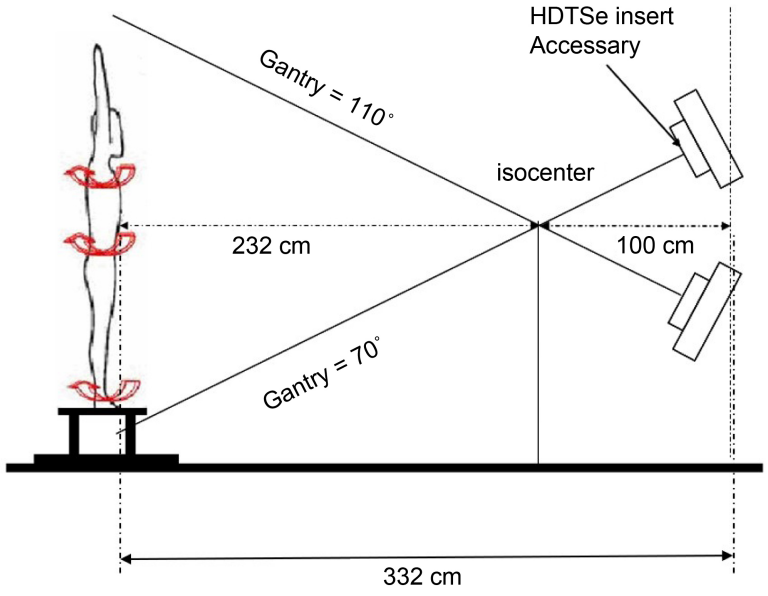

Figure 1. Provides a schematic view of the treatment geometry for dual field rotational total skin electron therapy (DFR-TSET) at a nominal Source-to-Skin Distance (SSD) of 232 + 100 = 332 cm. The figure illustrates the setup configuration for the treatment, showing the positioning of the patient and the treatment machine.

of 600 MU/min typically required approximately 30 minutes, with 15 minutes allocated for patient set-up and 15 minutes for the beam-on time to deliver the prescribed dose.

During treatment, the patient's eyes were shielded internally, and nails and toes were shielded externally. Commercial tungsten eye shields (3 mm tungsten coated with 1 mm aluminum) were used for eye shielding [31]. Lead sheets with a thickness of 3 mm were used to shield the nails and toes after delivering a dose of 12.5 Gy [32].

2.2. Dosimetry Measurements

Dosimetry measurements included 1) measuring the static dose rate at the extended SSD, 2) rotational dose rate for a rotating phantom, and 3) a correction to individual field profile for SSD variation over the skin surface.

1) Static Measurements: Static measurements were performed at an SSD of 332 cm using a NACP parallel plate ionization chamber in a polystyrene phantom. The measurements were carried out in a 10 × 10 cm^2 field at an isocenter SSD of 100 cm for a single horizontal 6 MeV beam. The dosimetry standard was used to calibrate the measurements.

2) Rotational Calibration: The rotational dose rate was measured by comparing the rotational dose to the static dose for one revolution at the extended SSD and phantom. The rotational correction factor was determined as the ratio of the rotational dose to the static dose.

3) Individual Field Profile: To determine the combined dose distribution of the dual field, the individual field profile was measured along the vertical direction using a parallel plate chamber. The measurements were performed for the beam with a gantry angle of 90˚ at the extended SSD. The composite dose profile was obtained by combining the individual beam profiles, matching the 50% dose line.

2.3. *In-Vivo* Dosimetry

In order to ensure safe and accurate radiation delivery to patients during RTSET treatment, *in-vivo* dose measurements were conducted using film, MOSFET, and optically stimulated luminescent dosimeter (OSLD).

1) Film Dosimetry: Kodak XV film (Kodak, Rochester, NY) was used for *in-vivo* dosimetry measurements. Film characteristics were obtained by exposing a series of films in a 10 × 10 cm^2 field at an SSD of 100 cm with doses ranging from 0 - 150 cGy. The films were analyzed using a densitometer to obtain dose-versus-reading data. The irradiated films were calibrated using a curve between densitometer reading and delivered dose. The film strips were securely attached to the patient's skin to ensure no air gaps.

2) MOSFET Dosimetry (Best Medical Canada, formerly Thomson and Nielsen Electronics Ltd., Ottawa, Ontario Canada): High-sensitivity MOSFET dosimeters, composed of two MOSFET devices mounted together, were used for *in-vivo*

surface dose measurements [33] [34] [35]. The dosimeters were calibrated with and without buildup for a 10 × 10 cm^2 static field at an SSD of 100 cm for 6 MeV electron beams.

3) OSLD Dosimetry: OSLD detectors, consisting of aluminum oxide doped with carbon, were used for *in-vivo* dose measurements (MicroStar Reader, Landauer, Inc., Glenwood, IL) [35] [36] [37]. Calibration curves were created by irradiating the OSLDs with a 6 MeV electron beam in a 10 × 10 cm^2 field at d_{max} (=1.4 cm) and an SSD of 100 cm with doses ranging from 0 - 150 cGy. Four nanoDot detectors were used for each calibration point, and dose points were monitored in a solid water phantom using a Farmer ionization chamber. The reader software processed the conversion directly to dose in cGy by taking into account all the calibration factors involved. In the *in-vivo* dosimetry measurements, each detector was read three times, and the average reading was used for each measurement point.

3. Results and Discussions

3.1. Patient Safety

The shielding for patient's eyes, nails, and toes during treatment was crucial to ensuring patient safety. An eye shields was commercially available to protect a patient's lens during radiation therapy. A tungsten eye shield was made from a millimeter thick anodized aluminum cap to reduce the electron backscatter to the eyelids. The effectiveness of 3 mm lead shielding to fingernails and toes was sufficient to provide adequate (95%) shielding for normal organ at 6 MeV electron beam. A soft bandage sheet on top of the lead sheet provided effective shielding reducing potential backscatter toward treated skin.

3.2. X-Ray Contaminations

X-ray bremsstrahlung contamination on the central axis of stationary electron beams, with nominal energies of 6 - 20 MeV, typically contributed between 1% to 7% of the maximum dose [2] [3]. Without precautions, this can result in a significant absorbed dose from x-ray contamination throughout the patient's body. The DFR-TSET technique utilized the dual angled electron fields to reduce x-ray contamination by directing the central axis away from the patient as shown in **Figure 1** [3] [4].

3.3. Beam Profiles

The beam profiles [29] [38] were measured using a parallel plate ionization chamber in the phantom. The dose distribution of a single field along the vertical direction was measured in 10 cm increments, and the data points are shown as diamond symbols in **Figure 2(a)**. To obtain a combined profile, the 50% dose line was matched at a position of z = 75 cm from the horizontal position, as shown in **Figure 2(b)**. The combined profile demonstrated a deviation uniformity of less than ±6%.

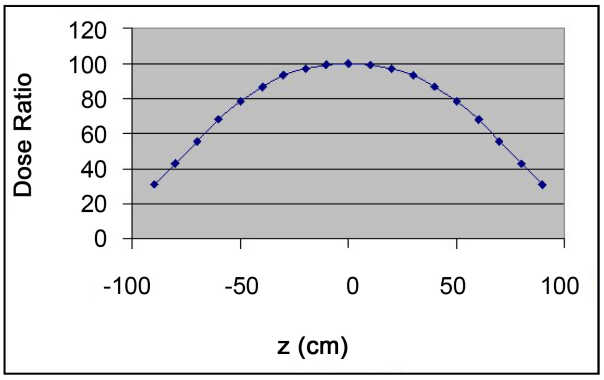

(a)

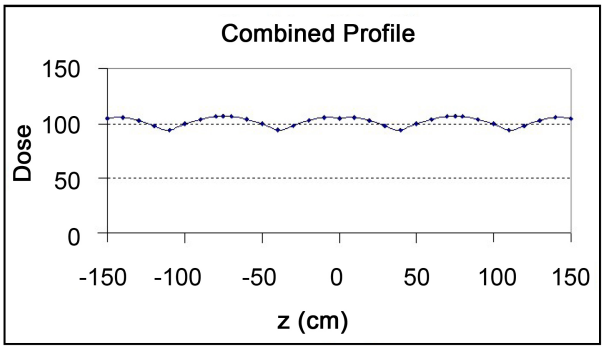

(b)

Figure 2. (a) Represents a single field vertical profile away from the horizontal position (z = 0). It shows the dose distribution along the vertical direction for a specific treatment field. The measured data points are indicated by diamond symbols on the graph. (b) Displays the combined profile for a Source-to-Skin Distance (SSD) of 332 cm. It is obtained by matching the 50% dose line at z = 75 cm using a combination of two beams. The gantry angles for these beams are 70˚ and 110˚, positioned at an equal angle of 20˚ above and below the horizontal position (gantry angle = 90˚). The combined profile illustrates the dose distribution achieved by combining the two beams.

3.4. Dosimetry

Regarding dosimetry characteristics, the static dose rate at a source-to-surface distance (SSD) of 332 cm was determined to be 0.0751 cGy/MU, based on comparison with the dose at SSD of 100 cm and a 10 × 10 cm^2 field. The rotational dose rate, which is the dose ratio of the static phantom at its d_{max} over the rotational phantom at its own d_{max}, was found to be 0.39 for one complete revolution at a machine rate of 600 MU/min.

Due to variations in the patient's abdomen thickness, the SSD correction was necessary. As electron beams do not follow an inverse square law, a power law correction was applied to account for SSD variations. In this setup, an empirically determined factor of 2.25 was used to describe this power law. Therefore, the dose to be delivered per revolution (DR) can be calculated using Equation

(1):

$$DR = DRs \times DRr \times \left(SSD_o / SSD\right)^p \times DRM \times Pr \quad (1)$$

where DRs is the static dose rate, DRr is the rotational rate ratio, SSD_o is the reference SSD (332 cm in this case), SSD is the patient-specific SSD, p is the power law factor, DRM is the machine rate, and Pr is the platform rotational rate.

Based on the measurements and setup described above, the following values were obtained:

DRs = 0.0751 cGy/MU;

DRr = 0.39;

p = 2.25;

Pr = 1/0.9 = 1.11 rpm.

For example, if a patient has an SSD of 325 cm and the machine rate is 600 MU/min, the dose per revolution can be calculated as follows:

DR = 0.0751 cGy/MU × $(332/325)^{2.25}$ × 0.39 × 600 (MU/min)/(1.11 rpm)

=16.6 cGy per revolution or 16.6 cGy per 540 MU (=32.53 MU/cGy).

If the prescription is 125 cGy per fraction, it would require approximately 7.5 revolutions, which is equivalent to 4066 MU. Since 7.5 revolutions is not an integer number, 7 and 8 revolutions were alternated every other day, resulting in delivered doses of 117 cGy and 133 cGy to the patient, respectively.

Charged Particle Equilibrium (CPE) status [39] may not be well established due to the use of extended SSDs for an electron beam. During static dose rate measurements at SSD of 332, a non-CPE feature was observed with the maximum depth dose moved to the surface in the percent depth dose (PDD) curve. We can use virtual SSD or effective SSD to describe electron beams. However, virtual SSDs might not provide accurate inverse square law corrections to the output of extended SSDs. Also, effective SSDs would vary with energy and field size, especially for extremely large field sizes [38]. Therefore, a modified power law was used to describe extended SSD differences between an individual patient and a calibrated phantom on the rotational platform. This power law deviated from the inverse square behavior by a factor of 2.25.

3.5. *In-Vivo* Dosimetry

In-vivo dosimetry measurements were performed during patient treatments to verify the delivered dose as prescribed and assess the uniformity of dose distribution [31]. *In vivo* dosimetry was a direct method of measuring radiation doses to patients receiving radiation treatment. It was a suitable method both to monitor treatment delivery, and to detect or prevent various errors early in course of treatment. Monitoring the dose delivery constituted a safety measure, being a part of the patient radiation protection. Moreover, the *in vivo* measurement provided a treatment record confirming that the dose was delivered correctly within the expected tolerance. Three different measurement methods were employed: XV film, MOSFET, and OSLD.

For XV film measurements, film strips were attached laterally across specific

regions of the patient's body, including the head, left arm, left anterior abdomen, left posterior thigh, left internal leg, and right calf. The prescribed dose for one patient per fraction was 116 cGy as shown in Figure 3(a), and the measured doses for these locations were as follows: 116 cGy, 104 cGy, 119 cGy, 108 cGy, 107 cGy, and 108 cGy, respectively. The maximum dose was observed on the abdomen (119 cGy), while the minimum dose was on the left arm (104 cGy), which was 94% of the maximum dose. The uniformity of the measured dose was within 6%, and the average measured dose was 110 cGy, approximately 5% lower than the prescribed dose.

In the case of MOSFET measurements, probes were attached to specific locations on the patient's body, including the neck, upper anterior abdomen, low anterior abdomen, and left posterior thigh. The prescribed dose to this patient was 125 cGy as shown in Figure 3(b), and the measured doses were 124 cGy, 124 cGy, 128 cGy, and 127 cGy, respectively. The measured doses ranged from 99% to 102% of the prescribed dose.

Both the film and MOSFET measurements indicated good dose uniformity and agreement between the delivered and prescribed doses in the dual field RTSET approach. These results supported the adequacy of the dosimetry calibration and treatment protocols. However, among the various detector types, OSLDs were found to have advantages over films and MOSFET in terms of better handling, quick reading, and exporting of measurement results. OSLDs also allowed for the use of multiple detectors due to their small size, enabling more precise dose distribution information during *in-vivo* dosimetry measurements.

OSLD detectors were attached across the patient's whole body as shown in Figure 4, and four patients were selected for the *in-vivo* measurements. The measured doses for different locations were summarized in Table 1. The prescription dose varied for each patient based on the physician's protocol.

Table 1. Measured doses by OSLD in cGy as a function of patient skin regions indicated in Figure 4.

No.	1, 2	3	4	5	6	7	8	9	10	14
Area	PA	PA2	Neck	Upp arm	Low arm	AP	Out thigh	Med thigh	Ankle	Head top
Pat 1	131	NA	110	NA	115	113	128	116	159	NA
Pat 2	143	142	157	79	NA	131	144	113	166	147
Pat 3*	131	131	NA	74	NA	NA	NA	87	NA	93
Pat 4	170	185	159	62	188	188	210	154	208	137

Remark: PA (Posterior-Anterior) is the reference point for dose calibration, indicating the patient's position in relation to the linear accelerator. PA2 is located 15 cm vertically above PA in the superior direction. AP (Anterior-Posterior) represents the calibration level on the anterior skin. NA (Not Available) indicates that data for this specific position is not provided.

In vivo dosimetry measurements using OSLDs were helpful in identifying underdosed regions that were blocked during treatment on the patient's skin [5] [37] [40]. Boost fields to local areas may be necessary based on clinical judgment

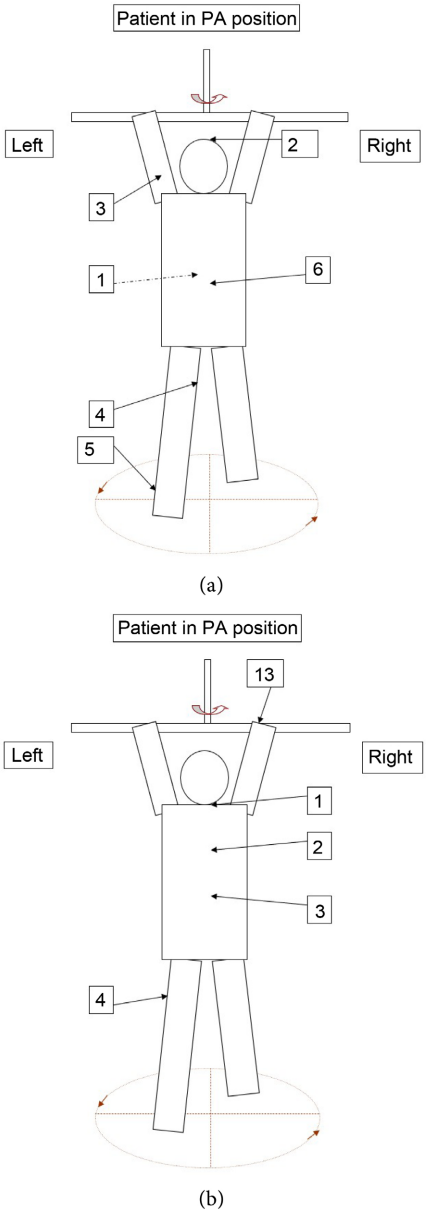

Figure 3. (a) Depicts a schematic view of *in-vivo* film dosimetry measurement for a patient in the posterior-anterior (PA) position. Film strips are attached laterally across various locations on the patient's body, including the head, left arm, left anterior abdomen, left posterior thigh, left internal leg, and right calf. The prescribed dose for this treatment is 116 cGy per fraction. The measured doses at these locations are provided, indicating the dose distribution achieved during the treatment. (b) Shows a schematic view of *in-vivo* MOSFET dosimetry measurement for a patient in the PA position. MOSFET probes are attached to the patient's neck, upper anterior abdomen, low anterior abdomen, and left posterior thigh. The prescribed dose for this treatment is 125 cGy per fraction. The measured doses at these locations are given, indicating the agreement between the delivered and prescribed doses.

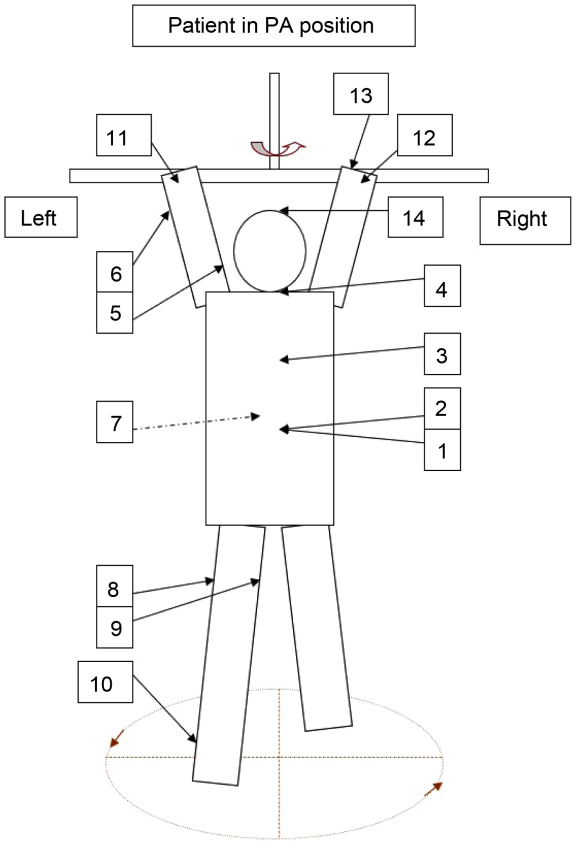

Figure 4. Displays a schematic view of *in-vivo* OSLD dosimetry measurement for a patient in the PA position. The figure shows the OSLD detectors attached across the patient's entire body, with specific numerical labels assigned to each detector location. **Table 1** provides information on the number of OSLD detectors used in relation to the patient's skin area. **Table 2** lists the prescription doses for the patients.

Table 2. OSLD dose reading versus blocked dose areas. The OSLD reading dose in all blocked areas is normalized to the prescription dose (Rx dose) and expressed as a percentage (%).

Patient No.	Rx dose (cGy)	Upper arm (%)	Top of head (%)	Medial thigh (%)
1	138	83.3	NA	92.8
2	137	58.4	NA	82.5
3	139	41.7	66.9	62.6
4	200	30.9	62.8	77
Average	NA	53.6	64.9	78.7

from the underdosed regions and their geometric sizes identified by the *in-vivo* OSLD results. OSLDs played an important role in providing the delivered dose distribution to avoid serious overdosing or underdosing when delivering the boost field. Boost local fields were delivered at conventional SSDs of 100-110 cm using standard electron cones and customized cutouts.

The specific regions requiring boost fields were not clearly defined and varied from one patient to another. OSLD *in-vivo* measurements assisted in identifying these regions. Generally, the boosted organ areas included the soles of the feet, the palms of the hands, the top of the head, and the upper parts of the arms in the outer region blocked by the head in DFR-TSET. These areas had already received certain doses from the RTSET treatment. The boost prescription dose would compensate for the partially delivered dose based on OSLD measurements during DFR-TSET.

A MOSFET dosimeter was being compared to OSLD in terms of their angular dependence for *in-vivo* skin dose measurements. A MOSFET dosimeter was based on a semiconductor material and exhibits an angular dependence in its response. The measured dose can vary depending on the angle at which the radiation beam interacts with the dosimeter. For *in-vivo* skin dose measurements, a MOSFET dosimeter showed a relatively high angular dependence of around 5% - 7% [34] or even higher, [35] indicating that the measured dose can significantly change with varying angles of incidence.

OSLDs also showed a small angular dependence. The reported angular dependence for OSLDs in the MeV energy range was about 3% - 4% [41]. This suggested that the measured dose with a OSLD detector was less affected by changes in the angle of beam incidence.

In the specific treatment scenario, DFR-TSET, where the patient was positioned in a rotational platform with a radiation beam on, the dose angular dependence appeared to be reduced. The rotational positioning would average out the effects of different incident angles, leading to an averaged effect in terms of surface dose absorption. This implied that the angular dependence of the dosimeter become less effective because the dose received on the skin was averaged over the patient rotation.

Overall, *in-vivo* skin dose measurements can exhibit certain directional dependencies. However, in the DFR-TSET technique, the angular dependence can be further minimized, resulting in an average effect. One potential reason for this was the rotational positioning of the patient during the delivery of the radiation beam, which tended to mitigate a specific angular effect.

4. Conclusions

In conclusion, the implementation of dual field rotational total skin electron therapy (DFR-TSET) has been successfully and clinically implemented. This technique, utilizing the special mode for electron beams in a medical linac, combines the benefits of the Stanford and McGill methods, including short beam-on times, uniform dose distributions, large treatment fields, and reduced x-ray contamination to patients. The measurements using film and MOSFET demonstrated a good agreement between the delivered dose and the prescribed dose. OSLD measurements proved to be crucial in identifying underdosed regions where boost fields were necessary to achieve the prescribed dose and ensure dose

uniformity along the patient's skin. OSLDs provided precise dose distribution information and facilitated the determination of boost areas. The results obtained from OSLD measurements supported the need for customization of treatment plans to address specific regions that may have received suboptimal doses during DFR-TSET.

The DFR-TSET technique has shown promising results in delivering accurate and uniform doses to patients undergoing total skin electron therapy. These advancements in dosimetry calibration and treatment protocols contribute to the improvement of patient care and treatment outcomes in radiation therapy.

Acknowledgements

The authors express gratitude to Dr. Glenn P. Glasgow, who passed away in 2019 for his encouragement and participation in this work, as well as colleagues in the Department of Radiation Oncology at Loyola University Medical Center in Maywood, Illinois, for their support and discussions.

Conflicts of Interest

Authors have no conflict of interest.

References

[1] Karzmark, C.J., Loevinger, R., Steele, R.E. and Weissbluth, M. (1960) A Technique for Large-Field, Superficial Electron Therapy. *Radiology*, **74**, 633-644. https://doi.org/10.1148/74.4.633

[2] Karzmark, C.J. (1964) Large-Field Superficial Electron Therapy with Linear Accelerators. *The British Journal of Radiology*, **37**, 302-305. https://doi.org/10.1259/0007-1285-37-436-302

[3] Karzmark, C.J., Anderson, J., Fessenden, F., Svensson, G., *et al*. (1988) Total Skin Electron Therapy (Technique and Dosimetry. AAPM Report #23, TG-30). American Institute of Physics, New York. https://doi.org/10.37206/22

[4] Das, I.J., Copeland, J.F. and Bushe, H.S. (1994) Spatial Distribution of Bremsstrahlung in a Dual Electron Beam Used in Total Skin Electron Treatments. *Medical Physics*, **21**, 1733-1738. https://doi.org/10.1118/1.597215

[5] El-Khatib, E., Hussein, S., Nikolic, M., *et al*. (1995) Variation of Electron Beam Uniformity with Beam Angulation and Scatterer Position for Total Skin Irradiation with the Stanford Technique. *International Journal of Radiation Oncology*, *Biology*, *Physics*, **33**, 469-474. https://doi.org/10.1016/0360-3016(95)00112-C

[6] Podgorsak, E.B., Pla, C., Pla, M., Lefebvre, P.Y. and Heese, R. (1983) Physical Aspects of a Rotational Total Skin Electron Irradiation. *Medical Physics*, **10**, 159-168. https://doi.org/10.1118/1.595296

[7] Pla, C., Heese, R., Pla, M. and Podgorsak, E.B. (1984) Calculation of Surface Dose in Rotational Total Skin Electron Irradiation. *Medical Physics*, **10**, 539-546. https://doi.org/10.1118/1.595524

[8] Podgorsak, E.B. and Podgorsak, M.B. (1999) Total Skin Electron Irradiation. *The Modern Technology of Radiation Oncology*, In Van Dyk, J., Ed., Medical Physics Publishing, Madison, 663.

[9] Williams, P.C., Hunter, R.D. and Jackson, S.M. (1979) Whole Body Electron Ther-

apy in Mycosis Fungoides—A Successful Translational Technique Achieved by Modification of an Established Linear Accelerator. *The British Journal of Radiology*, **52**, 302-307. https://doi.org/10.1259/0007-1285-52-616-302

[10] Nien, H.H., Hsieh, C.H., Shueng, P.W. and Tien, H.J. (2023) Total Skin Treatment with Helical Arc Radiotherapy. *International Journal of Molecular Sciences*, **24**, Article No. 4492. https://doi.org/10.3390/ijms24054492

[11] Harrison, C., Young, J., Navi, D., Riaz, N., Lingala, B., Kim, Y. and Hoppe, R. (2011) Revisiting Low-Dose Total Skin Electron Beam Therapy in Mycosis Fungoides. *International Journal of Radiation Oncology*, *Biology*, *Physics*, **81**, e651-e657. https://doi.org/10.1016/j.ijrobp.2011.01.023

[12] Miao, T., Zhang, R., Jermyn, M., Bruza, P., Zhu, T., Pogue, B.W., Gladstone, D.J. and Williams, B.B. (2022) Computational Dose Visualization & Comparison in Total Skin Electron Treatment Suggests Superior Coverage by the Rotational versus the Stanford Technique. *Journal of Medical Imaging and Radiation Sciences*, **53**, 612-622. https://doi.org/10.1016/j.jmir.2022.08.006

[13] Diamantopoulos, S., Platoni, K., Dilvoi, M. and Nazos, I. (2011) Clinical Implementation of Total Skin Electron Beam (TSEB) Therapy: A Review of the Relevant Literature. *Physica Medica*, **27**, 62-68. https://doi.org/10.1016/j.ejmp.2010.09.001

[14] Piotrowski, T., Milecki, P., Skórska, M. and Fundowicz, D. (2013) Total Skin Electron Irradiation Techniques: A Review. *Advances in Dermatology and Allergology*, **30**, 50-55. https://doi.org/10.5114/pdia.2013.33379

[15] Chowdhary, M., Chhabra, A.M., Kharod, S. and Marwaha, G. (2016) Total Skin Electron Beam Therapy in the Treatment of Mycosis Fungoides: A Review of Conventional and Low-Dose Regimens. *Clinical Lymphoma*, *Myeloma and Leukemia*, **16**, 662-671. https://doi.org/10.1016/j.clml.2016.08.019

[16] Piotrowski, T. and Malicki, J. (2006) The Rotary Dual Technique for Total Skin Irradiation in the Treatment of Mycosis Fungoides. *Reports of Practical Oncology and Radiotherapy*, **11**, 29-37. https://doi.org/10.1016/S1507-1367(06)71047-1

[17] Canu, D., Pham-Ledard, A., Ouhabrache, N. and Beylot-Barry, M. (2022) Changes in Total Skin Electron Beam Therapy Modalities for Mycosis Fungoides: A Single-Centre Study. *Annales de Dermatologie et de Vénéréologie*, **149**, 180-184. https://doi.org/10.1016/j.annder.2022.02.006

[18] Smits, K., Quint, K.D., Vermeer, M.H., Daniëls, L.A., Willemze, R., Jansen, P.M., Jansen, W.P.A. and Neelis, K.J. (2022) Total Skin Electron Beam Therapy for Cutaneous T-Cell Lymphomas in the Netherlands: A Retrospective Analysis of Treatment Outcomes and Selection for High or Low Dose Schedule. *Clinical and Translational Radiation Oncology*, **33**, 77-82. https://doi.org/10.1016/j.ctro.2021.12.001

[19] Morris, S., Scarisbrick, J., Frew, J., Irwin, C., Grieve, R., Humber, C., Kuciejewska, A., Bayne, S., Weatherhead, S., Child, F., Wain, M. and Whittaker, S. (2017) The Results of Low-Dose Total Skin Electron Beam Radiation Therapy (TSEB) in Patients with Mycosis Fungoides from the UK Cutaneous Lymphoma Group. *International Journal of Radiation Oncology*, *Biology*, *Physics*, **99**, 627-633. https://doi.org/10.1016/j.ijrobp.2017.05.052

[20] Xie, Y., Petroccia, H., Maity, A., Miao, T., Zhu, Y., Bruza, P., Pogue, B.W., Plastaras, J.P., Dong, L. and Zhu, T.C. (2020) Cherenkov Imaging for Total Skin Electron Therapy (TSET). *Medical Physics*, **47**, 201-212. https://doi.org/10.1002/mp.13881

[21] Ding, G.X., Osmundson, E.C., Shinohara, E., Newman, N.B., Price, M. and Kirschner, A.N. (2021) Monte Carlo Study on Dose Distributions from Total Skin

Electron Irradiation Therapy (TSET). *Physics in Medicine & Biology*, **66**, Article ID: 075010. https://doi.org/10.1088/1361-6560/abedd7

[22] Ding, G.X. (2021) Stopping-Power Ratios for Electron Beams Used in Total Skin Electron Therapy. *Medical Physics*, **48**, 5472-5478. https://doi.org/10.1002/mp.15121

[23] Elsayad, K., Weishaupt, C., Moustakis, C., Danzer, M.F., Müller, E.C., *et al*. (2023) Ultrahypofractionated Low-Dose Total Skin Electron Beam in Advanced-Stage Mycosis Fungoides and Sézary Syndrome. *International Journal of Radiation Oncology, Biology, Physics*, **117**, 164-170. https://doi.org/10.1016/j.ijrobp.2023.02.052

[24] Elmahmoud, Z., Gunther, J.R. and Christopherson, K. (2023) A Simple Solution to Create a Custom Scalp-Sparing Helmet to Prevent Alopecia in Patients Undergoing Total Skin Electron Beam Therapy for Cutaneous T Cell Lymphoma. *Clinical and Translational Radiation Oncology*, **38**, 53-56. https://doi.org/10.1016/j.ctro.2022.10.005

[25] Newman, N.B., Patel, C.G., Ding, G.X., Zic, J.A., Zwerner, J., Osmundson, E.C. and Kirschner, A.N. (2021) Prospective Observational Trial of Low-Dose Skin Electron Beam Therapy in Mycosis Fungoides Using a Rotational Technique. *Journal of the American Academy of Dermatology*, **85**, 121-127. https://doi.org/10.1016/j.jaad.2020.12.023

[26] Kumar, P.P., Good, R.R., Jones, E.O., McAnulty, B.E. and Reeves, M.A. (1987) Dual-Field Rotational Technique for Total-Skin Electron-Beam Therapy. *American Journal of Clinical Oncology*, **10**, 344-354. https://doi.org/10.1097/00000421-198708000-00018

[27] Heumann, T.R., Esiashvili, N., Parker, S., Switchenko, J.M., Dhabbaan, A., Goodman, M., Lechowicz, M.J., Flowers, C.R. and Khan, M.K. (2015) Total Skin Electron Therapy for Cutaneous T-Cell Lymphoma Using a Modern Dual-Field Rotational Technique. *International Journal of Radiation Oncology, Biology, Physics*, **92**, 183-191. https://doi.org/10.1016/j.ijrobp.2014.11.033

[28] Peters, V.G. and Jaywant, S.M. (1995) Implementation of Total Skin Electron Therapy Using an Optional High Dose Rate Mode on a Conventional Linear Accelerator. *Medical Dosimetry*, **20**, 99-104. https://doi.org/10.1016/0958-3947(95)00013-M

[29] Chen, Z., Agostinelli, A.G., Wilson, L.D. and Nath, R. (2004) Matching Dosimetry Characteristics of a Dual-Field Stanford Technique to a Customized Single-Field Stanford Technique for Total Skin Electron Therapy. *International Journal of Radiation Oncology, Biology, Physics*, **59**, 872-885. https://doi.org/10.1016/j.ijrobp.2004.02.046

[30] Varian Medical System (2012) Clinac Technical Reference Guide. Version 9.1, PN 100054117-03, 101-102.

[31] Fraass, B.A., Roberson, P.L. and Glatstein, E. (1983) Whole-Skin Electron Treatment: Patient Skin Dose Distribution. *Radiology*, **146**, 811-814. https://doi.org/10.1148/radiology.146.3.6828698

[32] Smeda, M.I., Johnston, D.O., Salzman, F.A., Trump, J.G. and Wright, K.A. (1962) Ten-Year Experience with Low Megavolt Electron Therapy. *The American Journal of Roentgenology Radium Therapy and Nuclear Medicine*, **88**, 215-228.

[33] Butson, M.J., Rozenfeld, A., Mathur, J.N., Carolan, M., Wong, T.Y. and Metcalfe, P.E. (1996) A New Radiotherapy Surface Dose Detector: The MOSFET. *Medical Physics*, **23**, 655-658. https://doi.org/10.1118/1.597702

[34] Qin, S., Chen, T., Wang, L., Tu, Y., Yue, N. and Zhou, J. (2014) Angular Depen-

dence of the MOSFET Dosimeter and Its Impact on *in Vivo* Surface Dose Measurement in Breast Cancer Treatment. *Technology in Cancer Research & Treatment*, **13**, 345-352. https://doi.org/10.7785/tcrt.2012.500382

[35] Consorti, R., Petrucci, A., Fortunato, F., Soriani, A., Marzi, S., Iaccarino, G., Landoni, V. and Benassi, M. (2005) *In Vivo* Dosimetry with MOSFETs: Dosimetric Characterization and First Clinical Results in Intraoperative Radiotherapy. *International Journal of Radiation Oncology*, *Biology*, *Physics*, **63**, 952-960. https://doi.org/10.1016/j.ijrobp.2005.02.049

[36] Jursinic, P.A. (2010) Changes in Optically Stimulated Luminescent Dosimeter (OSLD) Dosimetric Characteristics with Accumulated Dose. *Medical Physics*, **37**, 132-140. https://doi.org/10.1118/1.3267489

[37] Akselrod, M.S., Kortov, V.S., Kravetsky, D.J. and Gotlib, V.I. (1990) High Sensitivity Thermoluminescent Anion-Defective Al_2O_3:C Crystal Detectors. *Radiation Protection Dosimetry*, **32**, 15-20. https://doi.org/10.1093/oxfordjournals.rpd.a080771

[38] Khan, F.M. and Gibbons, J.P. (2014) The Physics of Radiation Therapy. 5th Edition, Lippincott Williams & Wilkins, Philadelphia.

[39] Attix, F.H. (1986) Introduction to Radiological Physics and Radiation Dosimetry. Wiley, New York. https://doi.org/10.1002/9783527617135

[40] Gaza, R., McKeveer, S.W.S., Akselrod, M.S., Akselrod, U.A.T., Yoder, C., Andersen, C.E., Aznar, M.C., Marckmann, C.J. and Bøtter-Jensen, L. (2004) A Fiber Dosimetry Method Based on OSL from Al_2O_3:C: for Radiotherapy Applications. *Radiation Measurements*, **38**, 809-812. https://doi.org/10.1016/j.radmeas.2003.12.004

[41] Mijnheer, B., Beddar, S., Izewska, J. and Reft, C. (2013) *In Vivo* Dosimetry in External Beam Radiotherapy. *Medical Physics*, **40**, Article ID: 070903. https://doi.org/10.1118/1.4811216